

# MODELING THE ALIGNMENT PROFILE OF SATELLITE GALAXIES IN CLUSTERS

Hyunmi Song and Jounghun Lee

*Astronomy Program, FPRD, Department of Physics and Astronomy, Seoul National University, Seoul 151-747, Korea*

hmsong@astro.snu.ac.kr, jounghun@astro.snu.ac.kr

## ABSTRACT

Analyzing the halo and galaxy catalogs from the Millennium simulations at redshifts  $z = 0, 0.5, 1$ , we determine the alignment profiles of cluster galaxies by measuring the average alignments between the major axes of the pseudo inertia tensors from all satellites within cluster's virial radius and from only those satellites within some smaller radius as a function of the top-hat scale difference. The alignment profiles quantify how well the satellite galaxies retain the memory of the external tidal fields after merging into their host clusters and how fast they lose the initial alignment tendency as the cluster's relaxation proceeds. It is found that the alignment profile drops faster at higher redshifts and on smaller mass scales. This result is consistent with the picture that the faster merging of the satellites and earlier onset of the nonlinear effect inside clusters tend to break the preferential alignments of the satellites with the external tidal fields. Modeling the alignment profile of cluster galaxies as a power-law of the density correlation coefficient that is independent of the power spectrum normalization ( $\sigma_8$ ) and demonstrating that the density correlation coefficient varies sensitively with the density parameter ( $\Omega_m$ ) and neutrino mass fraction ( $f_\nu$ ), we suggest that the alignment profile of cluster galaxies might be useful for breaking the  $\Omega_m$ - $\sigma_8$  and  $f_\nu$ - $\sigma_8$  degeneracies.

*Subject headings:* cosmology:theory — large scale structure of Universe

## 1. INTRODUCTION

The most salient feature of the large scale structure in the Universe is the web-like filamentary pattern of the spatial distribution of the galaxies, which is often referred to

as the cosmic web (Bond et al. 1996). Ever since the work of Hawley & Peebles (1975) who proposed testing the statistical significance of the anisotropy in the orientations of the galaxies embedded in the large-scale structure, plenty of observational and numerical researches have been conducted to understand the origin, property and dynamics of the cosmic web within the basic framework of the standard  $\Lambda$ CDM ( $\Lambda$ +cold dark matter) cosmology (e.g., West 1989; West et al. 1991; Schmalzing et al. 1999; Erdoğdu et al. 2004; Colberg et al. 2005; Dolag et al. 2006; Shen et al. 2006; Faucher-Giguère et al. 2008; Forero-Romero et al. 2009; Zhang et al. 2009; Shandarin et al. 2010; Gay et al. 2010; Aragón-Calvo et al. 2010a,b; Bond et al. 2010; Murphy et al. 2011; Noh & Cohn 2011; Shandarin 2011; Sousbie 2011; Vera-Ciro et al. 2011).

It is now understood that the anisotropic spatial correlations of the gravitational tidal fields mould the large scale structure into the cosmic web (e.g., Altay et al. 2006; Wang et al. 2011), which interconnects the Universe on different scales and translates the large-scale anisotropy into the small-scale intrinsic alignments (e.g., Binggeli 1982; West et al. 1991, 1995; Bond et al. 1996; Colberg et al. 1999; Pen et al. 2000; West & Blakeslee 2000; Plionis & Basilakos 2002; Knebe et al. 2004; Navarro et al. 2004; Zentner et al. 2005; Faltenbacher et al. 2005; Lee et al. 2005; Bailin & Steinmetz 2005; Colberg et al. 2005; Kasun & Evrard 2005; Hahn et al. 2007; Lee & Evrard 2007; Faltenbacher et al. 2008; Lee et al. 2009; Faltenbacher et al. 2009; Niederste-Ostholt et al. 2010; Paz et al. 2011; Wang et al. 2011; Lee 2011).

Many observational phenomena can attribute to the interconnection between the large-scale anisotropy and the small-scale intrinsic alignments. For instance, Godłowski & Flin (2010) reported the detection of strong correlations between the orientations of the galaxy groups and the neighbor group distributions on the scale up to  $20 h^{-1}\text{Mpc}$ . Paz et al. (2011) found a strong alignment signal between the projected major axes of the group shapes and the surrounding galaxy distribution up to scales of  $30 h^{-1}\text{Mpc}$ . They noted that this observed anisotropy signal becomes larger as the galaxy group mass increases, which is in excellent agreement with the prediction of the  $\Lambda$ CDM cosmology. Their result is also consistent with the previous findings that the degree of the alignment of the cluster galaxies depends on the velocity dispersion and number of the cluster galaxies (Plionis et al. 2003; Aryal et al. 2007; Godłowski et al. 2010; Godłowski 2011b). Smargon et al. (2011) detected a weak signal of the alignments between the projected major axes of the neighbor clusters on the scale of  $20 h^{-1}\text{Mpc}$  as well as a strong signal of the alignments between the cluster major axis and the direction to the other clusters on scales up to  $100 h^{-1}\text{Mpc}$ . (see also Hashimoto et al. 2008; Wang et al. 2009; Hao et al. 2011; Schaefer & Merkel 2011). Trujillo et al. (2006) and Varela et al. (2012) found that the spin axes of the spiral galaxies in the vicinity of the voids tend to lie on the surfaces of the voids, while Jones et al. (2010) showed that the spin axes of the spiral galaxies located in the cosmic filaments tend to be aligned with the elongated

axes of the host filaments. For a comprehensive review on the issue of the galaxy orientation and its relation to the structure formation, see Schäfer (2009) and Godłowski (2011a).

According to the previous works, the nonlinear evolution of the gravitational tidal fields has dual effects. On the one hand it sharpens the cosmic web and enhances the degree of the large-scale anisotropy by inducing filamentary merging and accretion. On the other hand it diminishes the interconnections between small and large scales by developing secondary filaments and local effects. To explain the formation and evolution of the large-scale structure in the cosmic web, it is first necessary to understand how the correlation of the tidal fields evolves in a scale dependent way. The galaxy clusters are the best target for investigating the evolution of the tidal connections between large and small scales. Often forming at the intersections of the filaments, the majority of the clusters are not isolated but in constant interactions with the surrounding large scale structure (e.g., Springel et al. 2005).

The anisotropic merging of satellites from the surroundings along the major filaments leads to the preferential locations of the satellite galaxies near the minor principal axes of the external tidal fields (i.e., the directions of the least compression). As the clusters become relaxed, however, the internal tidal fields develop into dominance, gradually rearranging the satellite distributions and deviating them from the directions of the external tidal fields. Those satellites which merged earlier, being located in the inner regions of the clusters, tend to become less aligned with the directions of the external tidal fields. In this picture, it may be expected that the profiles of the alignments between the spatial distributions of the satellites in the inner and the outermost regions of the clusters reflect how dominant the dark matter is and how fast the clusters grow in the Universe (e.g., see Colberg et al. 2005; Altay et al. 2006; Wang et al. 2011; Lee 2010; Baldi et al. 2011).

Here, we determine the alignment profile of cluster galaxies using the numerical data from a large N-body simulation and construct a theoretical model for it. The organization of this paper is as follows. In §2, the numerical datasets from N-body simulations are described and the alignment profiles of the cluster galaxies for the three and two dimensional cases are determined. In §3, a theoretical model for the alignment profile of the cluster galaxies is presented and fitted to the numerical results. In §4, we discuss the possibility of using the alignment profile of cluster galaxies as a cosmological probe. In §5, the results are summarized and a final conclusion is reached.

## 2. DATA AND ANALYSIS

We use the semi-analytic galaxy catalogs as well as the halo catalogs<sup>1</sup> at  $z = 0, 0.5$  and  $1$  from the Millennium Simulation for a  $\Lambda$ CDM concordance cosmology with  $\Omega_m = 0.25$ ,  $\Omega_\Lambda = 0.75$ ,  $h = 0.73$ ,  $n_s = 1.0$ ,  $\sigma_8 = 0.9$  (Springel et al. 2005). The dark matter halos and their substructures in the catalogs were found with the help of the standard friends-of-friends (FOF) and SUBFIND algorithms (Springel et al. 2001), respectively, while the galaxies in the semianalytic catalogs were modeled according to the merger trees derived from the semi-analytic simulations of the galaxy formation (Croton et al. 2006).

For the cluster halos with mass larger than  $10^{14} h^{-1} M_\odot$  at each redshift, we locate their satellite galaxies from the semi-analytic galaxy catalog and measure the pseudo inertia tensor,  $(I_{ij})$ , defined in terms of the relative positions of the satellite galaxies located within cluster’s virial radius  $r_{vir}$  as

$$I_{ij}(r_{vir}) = \sum_{x_\alpha \leq r_{vir}} x_{\alpha,i} x_{\alpha,j}, \quad (1)$$

where  $\mathbf{x}_\alpha = (x_{\alpha,i})$  is the position vector of the  $\alpha$ -th satellite relative to the halo center and  $x_\alpha \equiv |\mathbf{x}_\alpha|$  is its magnitude. Diagonalizing  $(I_{ij})$ , we find the three eigenvalues and corresponding unit eigenvectors of the pseudo inertia tensor for each cluster halo. We select only those clusters which satisfy  $(\varrho_3/\varrho_1)^{1/2} < 0.9$  where  $\lambda_3$  and  $\lambda_1$  are the smallest and the largest eigenvalues of  $I_{ij}(r_{vir})$ , expecting their pseudo inertia tensors to have three distinct eigenvectors. For each selected cluster halo, the major axis at the virial radius,  $\mathbf{e}(r_{vir})$ , is determined as the unit eigenvector corresponding to  $\varrho_1$ .

Using only those satellites located within some radial distance smaller than the cluster’s virial radius,  $r < r_{vir}$ , we recalculate the pseudo inertia tensor of each cluster’s interior region measured at  $r$ ,

$$I_{ij}(r) = \sum_{x_\alpha \leq r} x_{\alpha,i} x_{\alpha,j}. \quad (2)$$

Diagonalizing  $I_{ij}(r)$  and determining its unit eigenvector corresponding to the largest eigenvalue, we find the major axis,  $\mathbf{e}(r)$ , at the radial distance  $r$ , of the interior region of each cluster. The square of the cosine of the angle between the two major axes is now calculated as  $\cos^2 \theta \equiv |\mathbf{e}(r_{vir}) \cdot \mathbf{e}(r)|^2$  for each selected cluster halo. Figure 1 illustrates the projected positions of the satellite galaxies in a selected cluster, showing how the alignment angle,  $\theta$ , between the distributions of the satellites located within two different radial distances,  $r_{vir}$  and  $r$  is measured. Varying the value of  $r$  from  $0.9r_{vir}$  down to some cutoff radial distance,

---

<sup>1</sup> They are available at <http://www.mpa-garching.mpg.de/millennium>.

$r_c$ , defined as the radial distance within which less than five satellites are located, we repeat the whole calculation.

Since we are going to relate the alignment profiles of cluster galaxies to the auto-correlations of the tidal fields smoothed on two different top-hat filtering scales (see §3), we would like to express  $\cos^2 \theta$  as a function of the top-hat scale difference rather than the radial difference  $r_{vir} - r$ . For a given mass  $M(\leq r)$  enclosed by the radial distance  $r$ , the corresponding top-hat radial scale,  $R$ , is obtained as  $R(\leq r) = [3M(\leq r)/(4\pi\bar{\rho})]^{1/3}$  where  $\bar{\rho}$  is the mean mass density of the Universe. Here, the mass,  $M(\leq r)$ , can be calculated through integrating the NFW density profile (Navarro et al. 1996, 1997) from 0 to  $r$ , as done in Klypin et al. (1999):

$$M(\leq r) = M_{vir} \frac{f(\tilde{r})}{f(c)}, \quad (3)$$

where  $\tilde{r} \equiv r/r_s$  and  $f(\tilde{r}) \equiv \ln(1 + \tilde{r}) - \tilde{r}/(1 + \tilde{r})$ . Here the virial mass  $M_{vir}$  is defined as  $M_{vir} = [(4\pi/3)\rho_c 200 r_{vir}^3]$  where  $\rho_c$  is the critical density at  $z$  and  $r_s$  is the scale radius, and  $c$  is the concentration parameter defined as  $c \equiv r_{vir}/r_s$ , depending on  $M_{vir}$  and  $z$  as (Klypin et al. 1999)

$$c \approx \frac{124}{1+z} \left( \frac{M_{vir}}{1h^{-1}M_\odot} \right)^{-0.084}. \quad (4)$$

From here on we express  $\cos^2 \theta$  as a function of  $\Delta R \equiv R_0 - R$ , where  $R_0$  and  $R$  are the top-hat filtering scales corresponding to  $M_{vir}$  at  $z = 0$  and  $M(\leq r)$ , respectively, which can be calculated from  $r_{vir}$  and  $r$ , by Equations (3)-(4). The alignment profile of cluster galaxies is now defined as  $\langle \cos^2 \theta \rangle(\Delta R) - 1/3$ , where the constant factor  $1/3$  is subtracted from the ensemble average since the value of the ensemble average will be  $1/3$  when there is no alignment between the major axes of the pseudo inertia tensors measured on two scales,  $R$  and  $R_0$  (Pen et al. 2000; Lee & Pen 2001).

To investigate how the alignment profile of cluster galaxies depends on the mass scale, we divide the selected clusters at  $z = 0$  into three samples (I, II and III) according to their masses and separately measure the alignment profiles from each sample. Table 1 lists the redshift, logarithmic mass range and number of the selected clusters belonging to each sample in its second, third and fourth columns, respectively. The left panel of Figure 2 plots the alignment profiles of cluster galaxies from the subsamples I, II, and III as open triangles, diamonds, and squares, respectively. The uncertainties associated with the numerical data points represent the Jackknife errors. We divide the simulation volume into eight subvolumes (the Jackknife resamples) each of which contains the same number of halos and then measure the alignment profile using the halos from each Jackknife resample, separately. The Jackknife errors are finally obtained as the one standard deviation scatter among the eight resamples

(Wall & Jenkins 2008). It is worth mentioning here that the alignment profile is plotted as a function of  $\Delta R/R_0$  rather than  $\Delta R$  (where  $R_0$  is the top-hat filtering scale corresponding to  $M_{vir}$  at  $z = 0$ ) to make a fair comparison of the results from the three samples which must have different values of  $R_0$ . As can be seen, there are clear signals of alignments in the small  $\Delta R$  section, but the alignment profiles drop gradually as  $\Delta R$  increases for all three cases. The overall amplitude of the alignment profile shows a weak tendency to increase as the cluster’s mass increases.

We also measure the alignment profiles of cluster galaxies at  $z = 0.5$  and 1 to investigate how the profiles change with redshift. The left panel of Figure 3 compares the three alignment profiles at  $z = 0, 0.5$  and 1 (open squares, triangles and diamonds, respectively), where the cluster’s masses lie in the narrow range of  $10^{14} \leq \log(M/[h^{-1}M_\odot]) \leq 10^{14.2}$ . As can be seen, there is a strong tendency that the alignment profiles at higher redshifts drop faster with  $\Delta R$ , which implies that at higher redshifts the satellites in the inner regions of the clusters tend to be less aligned with the external tidal fields.

Recalling that what we can readily observe and measure is the two dimensional spatial distributions of the cluster galaxies rather than the three dimensional ones, we also measure the alignment profiles of cluster galaxies in the two-dimensional projected space. Adopting the flat-sky approximation and taking the  $z$ -axis as the line-of-sight direction, we project the positions of all satellites onto the  $x$ - $y$  plane and follow the exactly same procedures to determine the two dimensional alignment profiles as  $\langle \cos^2 \theta \rangle (R - R_0) - 1/2$  where the constant term  $1/2$  represents the case of no alignment for the two dimensional case. The left panels of Figures 4 and 5 plot the same as the left panels of Figures 2 and 3, respectively, but for the two dimensional case. As can be seen, the overall shapes and behaviors of the two dimensional alignment profiles are quite similar to the three dimensional ones except for the decrement of the amplitudes.

It is worth mentioning here that we evaluate the pseudo inertia tensors for the derivation of the cluster galaxy alignment profile (Eqs.[1]-[2]) rather than the conventional mass-weighted ones (e.g., Allgood et al. 2006), given that the pseudo inertia tensors have been found to quantify well the anisotropy in the galaxy spatial distribution caused by the local tidal fields (e.g., Shandarin et al. 2006; Park & Lee 2007). Since the calculation of the pseudo inertia tensors does not require any information on the satellite masses, the two dimensional alignment profile of the cluster galaxies is indeed a readily measurable quantity. In the following section, we provide physical explanations for the numerical results obtained here and present an analytic formula for the alignment profiles of cluster galaxies.

### 3. A THEORETICAL MODEL

Assuming that the alignment profiles of satellite galaxies in clusters are directly related to the spatial correlations of the tidal fields, we first measure the alignments between the minor principal axes of the tidal fields smoothed on two different scales, using the numerical data of the Millennium density fields constructed on  $256^3$  grids. As done in Lee & Erdogdu (2007), we perform the Fourier transform of the Millennium density field  $\delta(\mathbf{x})$  on each grid with the help of the FFT (Fast Fourier Transformation) method (Press et al. 1992) and calculate the Fourier transform of the tidal tensor smoothed on a given scale  $R_0$  as  $T_{ij}(\mathbf{k}) = k_i k_j \delta(\mathbf{k}) W(kR_0)/k^2$  where  $\mathbf{k} \equiv (k_i)$  is the wave vector and  $W(kR_0)$  is the top-hat window with the filtering radius  $R_0$ . The inverse Fourier transform of  $T_{ij}(\mathbf{k})$  gives the real space tidal field  $T_{ij}(\mathbf{x})$  smoothed on the scale of  $R_0$  at each pixel point. The unit eigenvector of  $T_{ij}(\mathbf{x})$  corresponding to the smallest eigenvalue represents the minor principal axis,  $\mathbf{u}(R_0)$ .

Repeating the whole process but smoothing the tidal field on some smaller scale  $R < R_0$ , we also determine the minor principal axis,  $\mathbf{u}(R)$ , of the tidal field on scale  $R$ . The alignment between the minor principal axes of the tidal fields smoothed on two different scales,  $R$  and  $R_0$ , is calculated as  $|\mathbf{u}(R) \cdot \mathbf{u}(R_0)|^2$  at each pixel. Varying the value of  $R$ , we repeat the whole calculation, average the alignments over  $256^3$  pixels and express the alignment profile of the minor axes of the tidal fields as a function of  $R_0 - R$ . Figure 6 plots  $\langle |\mathbf{u}(R) \cdot \mathbf{u}(R_0)|^2 \rangle$  at  $z = 0$  as open squares with  $R_0 = 8.7 h^{-1} \text{Mpc}$ . As can be seen, as  $R$  decreases, the strength of the alignment gradually decreases.

It was Lee & Pen (2001) who have for the first time shown that the auto-correlations between the principal axes of the linear tidal fields smoothed on two different scales can be approximated as a square-root of the density correlation coefficient,  $\xi(R_0 - R)$ , defined as (see also Lee et al. 2009)

$$\xi(R_0 - R) = \frac{\langle \delta_R \delta_{R_0} \rangle}{\sigma_R \sigma_{R_0}}, \quad (5)$$

$$\langle \delta_R \delta_{R_0} \rangle \equiv \int P(k) W(kR) W(kR_0) d^3 \mathbf{k}, \quad (6)$$

$$\sigma_R^2 \equiv \int P(k) W^2(kR) d^3 \mathbf{k}, \quad (7)$$

$$\sigma_{R_0}^2 \equiv \int P(k) W^2(kR_0) d^3 \mathbf{k}. \quad (8)$$

Adopting the model of Lee & Pen (2001) and extending it to the nonlinear regime, we approximate the spatial correlations of the minor principal axes of the nonlinear tidal fields smoothed on the two scales of  $R_0$  and  $R$  as

$$\langle |\mathbf{u}(R) \cdot \mathbf{u}(R_0)|^2 \rangle = \xi^\beta(R_0 - R), \quad (9)$$

where the power-law index,  $\beta$ , is an adjustable parameter. In the original work of Lee & Pen (2001), the linear power spectrum is used for the evaluation of the density correlation coefficient,  $\xi(R_0 - R)$ , through Equations (5)-(8). In our work, however, we redefine  $\xi(R_0 - R)$  in terms of the *nonlinear* density power spectrum instead of the linear power spectrum to account for the fact that the alignment profiles of cluster galaxies lie in the nonlinear regime. For the calculation of the nonlinear power spectrum, we adopt the analytic formula provided by Saito et al. (2008).

Adjusting the value of  $\beta$ , we fit the numerical results to Equation (9) via the standard  $\chi^2$ -minimization. The solid and dashed curves in Figure 6 represent the best-fit models for the cases that the nonlinear and linear density power spectrum are used for the calculation of  $\xi$ , respectively. Figure 6 shows that the alignments between the minor principal axes of the tidal fields on different scales are indeed well approximated as a power-law of the density correlation coefficient especially in the large  $\Delta R \equiv R_0 - R$  section and that the density correlation coefficient expressed in terms of the nonlinear power spectrum yields a better fit to the numerical results. The discrepancy between the numerical results and the best-fit analytic curves in the small- $\Delta R$  section ( $\Delta R \leq 4 h^{-1}\text{Mpc}$ ) should be attributed to the low-resolution of the Millennium tidal fields ( $256^3$  grids on a periodic box of linear size  $500 h^{-1}\text{Mpc}$ ).

As the alignments between the minor principal axes of the tidal fields on two different scales are now found to scale as a power-law of the density correlation coefficient, we model the three dimensional alignment profile of cluster galaxies as

$$\langle \cos^2 \theta \rangle - \frac{1}{3} = A \xi^n(\Delta R), \quad (10)$$

where the amplitude  $A$  and the power-law index  $n$  are two adjustable parameters, quantifying how strongly the satellites are aligned with the external tidal fields at the virial radius and how fast the alignment profile drops with  $\Delta R$ , respectively. Adjusting the values of  $A$  and  $n$ , we fit the numerical results presented in §2 to Equation (10) at each redshift. For the two dimensional case, the constant term in Equation (10) is changed from  $1/3$  to  $1/2$ . For the fitting model, we use the density correlation coefficient,  $\xi(\Delta R)$ , expressed in terms of the nonlinear density power spectrum and set the value of  $R_0$  at the maximum top-hat scale found from the clusters belonging to each sample.

The best-fit values of  $A$  and  $n$  are determined through minimizing the following generalized  $\chi^2$  (Hartlap et al. 2007):

$$\chi^2 = \sum_{i,j} \Delta \cos^2 \theta_i C_{ij}^{-1} \Delta \cos^2 \theta_j, \quad (11)$$

where  $\Delta \cos^2 \theta_i$  denotes the difference between the numerical result and the analytic model (Eq.[10]) at the  $i$ -th bin, and  $(C_{ij})$  is the covariance matrix defined as  $C_{ij} \equiv \langle (\cos^2 \theta_i - \langle \cos^2 \theta_i \rangle)(\cos^2 \theta_j - \langle \cos^2 \theta_j \rangle) \rangle$ , where the ensemble average is taken over the eight Jackknife resamples (see §2). The value of  $R_0$  for the best-fit analytic model is set at the maximum top-hat scale calculated from the masses of the clusters belonging to each sample.

The best-fit amplitude and power-law index for the three and two dimensional cases are listed in Tables 1-2. The uncertainties in the measurement of the best-fit parameter values represent the marginalized errors computed as the curvature of  $\chi^2$  at its minimum (Bevington & Robinson 1996; Wall & Jenkins 2008). Figures 2-5 plot the best-fit models as a function of  $1 - R/R_0$  in the left panels, which reveal that our analytic models (Eq.[10]) are indeed in good agreements with the numerical results for all cases. We also plot the same alignment profiles versus  $\xi(\Delta R)$  in the right panels of Figures 2-5 to show explicitly that the alignment profiles scale as a power-law of the density correlation coefficient.

The fitting results also show qualitatively how the alignment profiles of cluster galaxies change with mass scale and redshift. As the cluster mass scale increases, the amplitude of the alignment profile increases slightly while its power-law index decreases significantly. As the redshift increases, the amplitude of the alignment profile shows little change but its power-law index increases considerably. This result indicates that the satellite galaxies located in the massive clusters at lower redshifts tend to be more strongly aligned on average with the external tidal fields. To test the statistical significance of the dependence of the alignment profile on  $\log M$  and  $z$ , we analyze a simple linear regression of the best-fit values of  $A$  and  $n$  listed in Tables 1-2 for the three subsamples: (I, II, III) and (I,IV,V), respectively. Table 3 which lists the slope,  $\alpha$ , of each linear model shows quantitatively that the dependences of  $n$  on  $\log M$  and  $z$  are both significant with  $|\alpha| > 1$  while the dependences of  $A$  on  $\log M$  and  $z$  are insignificant.

The strong dependence of  $n$  on  $z$  can be explained as follows. At higher redshifts, the relative dominance of the dark matter density parameter,  $\Omega_m(z)$  is greater and thus the nonlinear effect inside the clusters would turn on earlier, resulting in higher degree of the deviation of the major axes of the pseudo inertia tensors of the cluster galaxies from the minor principal axes of the external tidal fields. As for the strong dependence of  $n$  on  $\log M$ , the more massive clusters are believed to form more recently and thus their relaxation process has yet to be completed. In consequence, the satellite galaxies of the more massive clusters would retain better memory of the preferential alignments with the minor principal axes of the external tidal fields. Meanwhile, the weak dependence of  $A$  on  $z$  and  $\log M$  may be interpreted as follows. The amplitudes of the alignment profiles are largely determined by the degree of the alignments of those satellite galaxies located at the virial radii of their

host clusters. Since those satellite are likely to have just merged into the clusters, they should always exhibit the strongest alignments with the external tidal fields, regardless of the redshift and mass scale.

It is worth mentioning here that our model for the alignment profile of cluster galaxies does not require precisely accurate measurement of the cluster’s virial radii, given that during the fitting procedure the value of  $R_0$  for our model is set at its maximum top-hat scale from the clusters belonging to each sample. In other words, the alignment profile of cluster galaxies can be constructed even when we have just approximate measurements of virial masses of the sample clusters.

#### 4. A COSMOLOGICAL IMPLICATION

Although we have considered only a single cosmological model to measure the alignment profile of cluster galaxies that lies in the non-linear regime, the strong redshift dependence of the alignment profile shown in §3 hints that it might depend on the background cosmology. Furthermore, the fact that the alignment profile scales as a power-law of the density correlation coefficient,  $\xi(\Delta R)$ , suggests that it might be useful for breaking the  $\Omega_m$ - $\sigma_8$  degeneracy since  $\xi(\Delta R)$  is independent of the power spectrum normalization  $\sigma_8$ .

To explore this possibility, we first examine how the density correlation coefficient,  $\xi(\Delta R)$ , changes with the matter density parameter. Varying the value of  $\Omega_m$  from 0.1 to 0.5 and fixing the other key cosmological parameters at the values used for the Millennium simulations, we repeatedly calculate  $\xi(\Delta R)$  expressed in terms of the nonlinear power spectrum (see §3), at  $z = 0$ , the results of which are plotted in the left panel of Figure 7. It reveals that the higher the value of  $\Omega_m$  is, the more rapidly the correlation coefficient  $\xi(\Delta R)$  drops with  $\Delta R$ . This result is consistent with our finding in §3 that the alignment profile of cluster galaxies drops faster with  $\Delta R$  at higher redshifts when the relative dominance of dark matter is high.

The other key cosmological parameter that we pay attention to is the neutrino mass,  $m_\nu$ . Recently, Marulli et al. (2011) have demonstrated by hydrodynamic simulations that if the neutrinos have non-zero mass (in a  $\Lambda$ CDM+ $\nu$  cosmology), then their free-streaming would have a strong impact on the formation and evolution of the large-scale structure, suppressing the formation of small- scale objects and thus decreasing the abundance of galaxy clusters and their clustering strength (see Lesgourgues & Pastor 2006, for a recent review). Yet, they emphasized that these effect caused by the neutrino free streaming are strongly degenerate with the power spectrum normalization factor,  $\sigma_8$ .

It is expected that if there are larger amount of free-streaming neutrinos, then they would defer the merging of the satellite galaxies into the clusters and thus the cluster galaxies would keep better the memory of the external tidal fields. The higher the fraction of massive neutrinos is, the higher amplitude and lower power-law index the alignment profile of cluster galaxies has. Under the speculation that our analytic model for a  $\Lambda$ CDM cosmology can be extended to  $\Lambda + \nu$ CDM cosmology, we calculate  $\xi(\Delta R)$  for five different cases of the neutrino mass fraction,  $f_\nu \equiv \Omega_\nu/\Omega_m$ . Regarding the nonlinear matter density power spectrum for a  $\Lambda$ CDM+ $\nu$  cosmology, we use the analytic formula provided by Saito et al. (2008). The right panel of Figure 7 plots the matter density correlation coefficient at  $z = 0$  for five different cases of  $f_\nu$ . The higher the value of  $f_\nu$  is, the correlation coefficient,  $\xi(\Delta R)$ , drops less rapidly with  $\Delta R$ , consistent with our expectation.

## 5. SUMMARY AND CONCLUSION

We have determined the three and two dimensional alignment profiles of cluster galaxies using the halo and semi-analytic galaxy catalogs from the Millennium simulation. The alignment profiles of cluster galaxies are defined as the average alignments between the major axes of the pseudo inertia tensors of the cluster galaxies on two different top-hat scales  $R_0$  and  $R$  (where  $R_0$  is the top-hat radius enclosing cluster’s virial mass and  $R < R_0$ ). The alignment profiles of cluster galaxies reflect how well the satellite galaxies, after merging into the clusters, retain the memory of the preferential alignments with the minor principal axes of the external tidal fields and how fast they gradually lose the alignment tendency under the influence of the internal tidal fields as the cluster’s relaxation proceeds and nonlinear effect becomes stronger.

It has been shown that the alignment profiles of cluster galaxies expressed as a function of  $\Delta R = R_0 - R$  behave as a power-law of the density correlation coefficient. The alignment profiles exhibit weak dependence of the amplitude  $A$  on mass scale and redshift but strong dependence of the power-law index  $n$  whose statistical significance is tested by using a simple linear regression analysis. As the cluster mass decreases and the redshift increases, the alignment profile drops faster with  $\Delta R$ , which is consistent with the scenario that the faster merging process of the satellites and earlier onset of the nonlinear effect inside the clusters tend to break more easily the preferential alignments of the cluster galaxies with the minor principal axes of the external tidal fields. The weak dependence of  $A$  on mass scale and redshift implies that the satellite galaxies located at the virial radii of their host clusters always keep good memory of the external tidal fields regardless of the mass scale and redshift.

We have suggested that the alignment profiles of cluster galaxies might be a complementary cosmological probe, being useful especially for breaking the  $\Omega_m$ - $\sigma_8$  and  $f_\nu$ - $\sigma_8$  degeneracies (where  $f_\nu$  is the neutrino mass fraction) owing to the insensitivity of  $\xi(\Delta R)$  to  $\sigma_8$ . To prove this theoretical concept, however, it will be necessary to test the validity of our model against N-body simulations for different cosmologies other than the  $\Lambda$ CDM model assumed for the Millennium simulations. As a large catalog of the galaxy clusters and their satellites from the Sloan Digital Sky Survey Data Release 7 is in the pipeline (Hao et al. 2010), our future work is in the direction of conducting numerical and observational tests of the alignment profiles of cluster galaxies presented here.

We thank an anonymous referee for the very useful comments and suggestions. The Millennium Simulation analyzed in this paper was carried out by the Virgo Supercomputing Consortium at the Computing Center of the Max-Planck Society in Garching, Germany. The simulation databases and the web application providing online access to them were constructed as part of the activities of the German Astrophysical Virtual Observatory. This work was supported by the National Research Foundation of Korea (NRF) grant funded by the Korea government (MEST, No.2011-0007819). Support for this work was also provided by the National Research Foundation of Korea to the Center for Galaxy Evolution Research.

## REFERENCES

- Allgood, B., Flores, R. A., Primack, J. R., Kravtsov, A. V., Wechsler, R. H., Faltenbacher, A., & Bullock, J. S. 2006, *MNRAS*, 367, 1781
- Altay, G., Colberg, J. M., & Croft, R. A. C. 2006, *MNRAS*, 370, 1422
- Aragón-Calvo, M. A., Platen, E., van de Weygaert, R., & Szalay, A. S. 2010, *ApJ*, 723, 364
- Aragón-Calvo, M. A., van de Weygaert, R., & Jones, B. J. T. 2010, *MNRAS*, 408, 2163
- Aryal, B., Paudel, S., & Saurer, W. 2007, *MNRAS*, 379, 1011
- Bailin, J., & Steinmetz, M. 2005, *ApJ*, 627, 647
- Baldi, M., Lee, J., & Macciò, A. V. 2011, *ApJ*, 732, 112
- Basilakos, S., Plionis, M., Yepes, G., Gottlöber, S., & Turchaninov, V. 2006, *MNRAS*, 365, 539
- Bevington, P. R. & Robinson, D. K. 1996, *Data Reduction and Error Analysis for the Physical Sciences* (Boston: McGraw-Hill)
- Binggeli, B. 1982, *A&A*, 107, 338
- Bond, J. R., Kofman, L., & Pogosyan, D. 1996, *Nature*, 380, 603
- Bond, N. A., Strauss, M. A., & Cen, R. 2010, *MNRAS*, 409, 156
- Bullock, J. S., Kolatt, T. S., Sigad, Y., Somerville, R. S., Kravtsov, A. V., Klypin, A. A., Primack, J. R., & Dekel, A. 2001, *MNRAS*, 321, 559
- Colberg, J. M., White, S. D. M., Jenkins, A., & Pearce, F. R. 1999, *MNRAS*, 308, 593
- Colberg, J. M., Krughoff, K. S., & Connolly, A. J. 2005, *MNRAS*, 359, 272
- Croton, D. J., et al. 2006, *MNRAS*, 365, 11
- Dolag, K., Meneghetti, M., Moscardini, L., Rasia, E., & Bonaldi, A. 2006, *MNRAS*, 370, 656
- Eisenstein, D. J., & Hu, W. 1999, *ApJ*, 511, 5
- Erdoğdu, P., et al. 2004, *MNRAS*, 352, 939

- Faltenbacher, A., Allgood, B., Gottlöber, S., Yepes, G., & Hoffman, Y. 2005, MNRAS, 362, 1099
- Faltenbacher, A., Jing, Y. P., Li, C., Mao, S., Mo, H. J., Pasquali, A., & van den Bosch, F. C. 2008, ApJ, 675, 146
- Faltenbacher, A., Li, C., White, S. D. M., Jing, Y.-P., Shu-DeMao, & Wang, J. 2009, Research in Astronomy and Astrophysics, 9, 41
- Faucher-Giguère, C.-A., Lidz, A., & Hernquist, L. 2008, Science, 319, 52
- Fisher, R. A. 1944, Statistical Methods for Research Workers (Oliver & Boyd)
- Forero-Romero, J. E., Hoffman, Y., Gottlöber, S., Klypin, A., & Yepes, G. 2009, MNRAS, 396, 1815
- Godłowski, W., & Flin, P. 2010, ApJ, 708, 920
- Godłowski, W., Piwowarska, P., Panko, E., & Flin, P. 2010, ApJ, 723, 985
- Godłowski, W. 2011, International Journal of Modern Physics D, 20, 1643
- Godłowski, W. 2011, arXiv:1110.2245
- Hahn, O., Carollo, C. M., Porciani, C., & Dekel, A. 2007, MNRAS, 381, 41
- Hao, J., et al. 2010, ApJS, 191, 254
- Hao, J., Kubo, J. M., Feldmann, R., et al. 2011, ApJ, 740, 39
- Hartlap, J., Simon, P., & Schneider, P. 2007, A&A, 464, 399
- Hashimoto, Y., Henry, J. P., & Boehringer, H. 2008, MNRAS, 390, 1562
- Hawley, D. L., & Peebles, P. J. E. 1975, AJ, 80, 477
- Jones, B. J. T., van de Weygaert, R., & Aragón-Calvo, M. A. 2010, MNRAS, 408, 897
- Kasun, S. F., & Evrard, A. E. 2005, ApJ, 629, 781
- Kazantzidis, S., Zentner, A. R., Kravtsov, A. V., Bullock, J. S., & Debattista, V. P. 2009, ApJ, 700, 1896
- Klypin, A., Gottlöber, S., Kravtsov, A. V., & Khokhlov, A. M. 1999, ApJ, 516, 530

- Gay, C., Pichon, C., Le Borgne, D., Teyssier, R., Sousbie, T., & Devriendt, J. 2010, MNRAS, 404, 1801
- Knebe, A., Gill, S. P. D., Gibson, B. K., Lewis, G. F., Ibata, R. A., & Dopita, M. A. 2004, ApJ, 603, 7
- Lee, J., & Pen, U.-L. 2001, ApJ, 555, 106
- Lee, J., Kang, X., & Jing, Y. P. 2005, ApJ, 629, L5
- Lee, J., & Evrard, A. E. 2007, ApJ, 657, 30
- Lee, J., & Erdogdu, P. 2007, ApJ, 671, 1248
- Lee, J., Springel, V., Pen, U.-L., & Lemson, G. 2008, MNRAS, 389, 1266
- Lee, J., Hahn, O., & Porciani, C. 2009, ApJ, 705, 1469
- Lee, J. 2010, arXiv:1008.4620
- Lee, J. 2011, ApJ, 732, 99
- Lesgourgues, J., & Pastor, S. 2006, Phys. Rep., 429, 307
- Marulli, F., Carbone, C., Viel, M., Moscardini, L., & Cimatti, A. 2011, arXiv:1103.0278
- Murphy, D. N. A., Eke, V. R., & Frenk, C. S. 2011, MNRAS, 413, 2288
- Navarro, J. F., Frenk, C. S., & White, S. D. M. 1996, ApJ, 462, 563
- Navarro, J. F., Frenk, C. S., & White, S. D. M. 1997, ApJ, 490, 493
- Navarro, J. F., Abadi, M. G., & Steinmetz, M. 2004, ApJ, 613, L41
- Niederste-Ostholt, M., Strauss, M. A., Dong, F., Koester, B. P., & McKay, T. A. 2010, MNRAS, 405, 2023
- Noh, Y., & Lee, J. 2007, ApJ, 666, 627
- Noh, Y., & Cohn, J. D. 2011, MNRAS, 413, 301
- Park, D., & Lee, J. 2007, Physical Review Letters, 98, 081301
- Paz, D. J., Sgró, M. A., Merchán, M., & Padilla, N. 2011, MNRAS, 502
- Pimblet, K. A. 2005, MNRAS, 358, 256

- Pen, U.-L., Lee, J., & Seljak, U. 2000, *ApJ*, 543, L107
- Plionis, M., & Basilakos, S. 2002, *MNRAS*, 329, L47
- Plionis, M., Benoist, C., Maurogordato, S., Ferrari, C., & Basilakos, S. 2003, *ApJ*, 594, 144
- Press, W. H., Teukolsky, S. A., Vetterling, W. T., & Flannery, B. P. 1992, Cambridge: University Press, —c1992, 2nd ed.
- Saito, S., Takada, M., & Taruya, A. 2008, *Physical Review Letters*, 100, 191301
- Schäfer, B. M. 2009, *International Journal of Modern Physics D*, 18, 173
- Schaefer, B. M., & Merkel, P. 2011, arXiv:1101.4584
- Schmalzing, J., Buchert, T., Melott, A. L., Sahni, V., Sathyaprakash, B. S., & Shandarin, S. F. 1999, *ApJ*, 526, 568
- Shandarin, S., Feldman, H. A., Heitmann, K., & Habib, S. 2006, *MNRAS*, 367, 1629
- Shandarin, S., Habib, S., & Heitmann, K. 2010, *Phys. Rev. D*, 81, 103006
- Shandarin, S. F. 2011, *Journal of Cosmology and Astroparticle Physics*, 5, 15
- Smargon, A., Mandelbaum, R., Bahcall, N., & Niederste-Ostholt, M. 2011, arXiv:1109.6020
- Shen, J., Abel, T., Mo, H. J., & Sheth, R. K. 2006, *ApJ*, 645, 783
- Sousbie, T. 2011, *MNRAS*, 414, 350
- Springel, V., White, S. D. M., Tormen, G., & Kauffmann, G. 2001, *MNRAS*, 328, 726
- Springel, V., et al. 2005, *Nature*, 435, 629
- Trujillo, I., Carretero, C., & Patiri, S. G. 2006, *ApJ*, 640, L111
- Varela, J., Betancort-Rijo, J., Trujillo, I., & Ricciardelli, E. 2012, *ApJ*, 744, 82
- Vera-Ciro, C. A., Sales, L. V., Helmi, A., et al. 2011, *MNRAS*, 416, 1377
- Villaescusa-Navarro, F., Miralda-Escudé, J., Peña-Garay, C., & Quilis, V. 2011, arXiv:1104.4770
- Wall, J. V., & Jenkins, C. R. 2008, *Practical Statistics for Astronomers*, (Cambridge:Cambridge University Press)

- Wang, Y., Park, C., Yang, X., Choi, Y.-Y., & Chen, X. 2009, *ApJ*, 703, 951
- Wang, H., Mo, H. J., Jing, Y. P., Yang, X., & Wang, Y. 2011, *MNRAS*, 413, 1973
- West, M. J. 1989, *ApJ*, 347, 610
- West, M. J., Villumsen, J. V., & Dekel, A. 1991, *ApJ*, 369, 287
- West, M. J., Jones, C., & Forman, W. 1995, *ApJ*, 451, L5
- West, M. J., & Blakeslee, J. P. 2000, *ApJ*, 543, L27
- Zhang, Y., Yang, X., Faltenbacher, A., Springel, V., Lin, W., & Wang, H. 2009, *ApJ*, 706, 747
- Zentner, A. R., Kravtsov, A. V., Gnedin, O. Y., & Klypin, A. A. 2005, *ApJ*, 629, 219

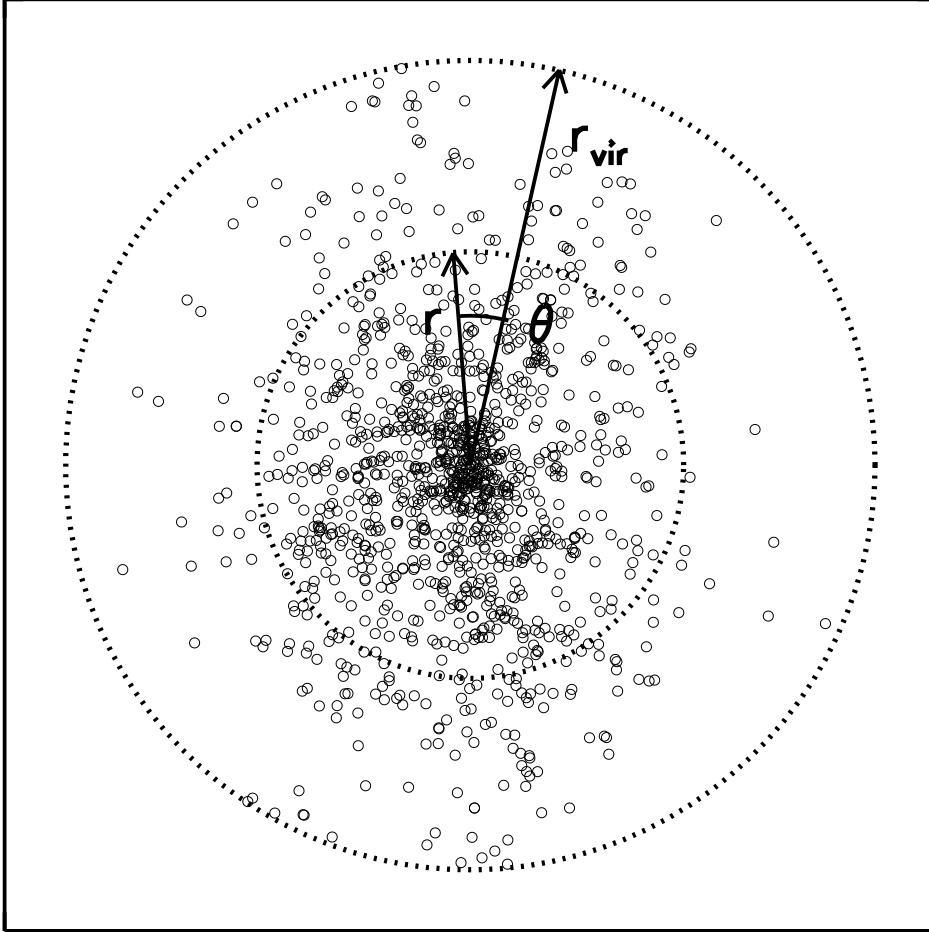


Fig. 1.— Illustration of the anisotropic spatial distributions of the satellite galaxies in the two dimensional projected plane and the angle  $\theta$  between the major axes of the pseudo inertia tensors of the satellites within two different radial distances.

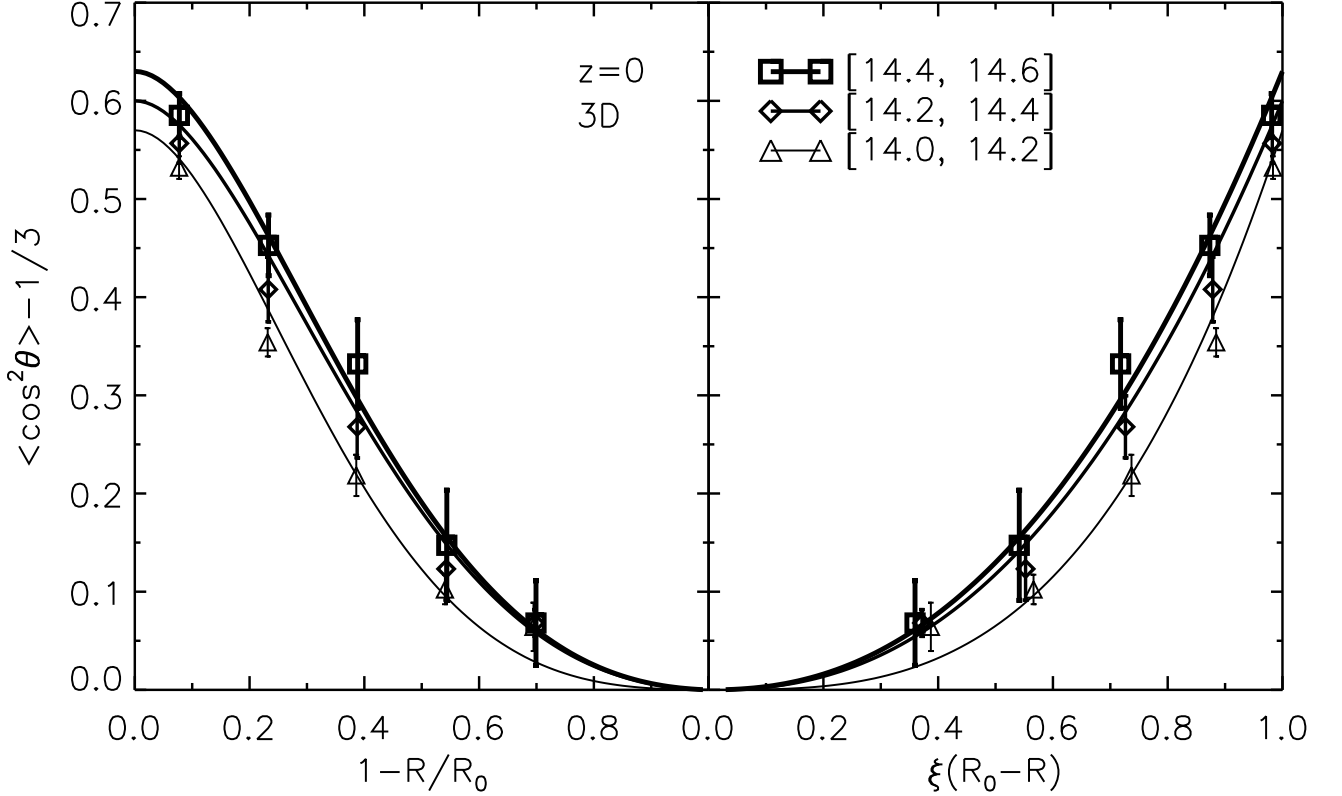


Fig. 2.— Three dimensional alignment profiles of satellite galaxies in cluster halos identified at  $z = 0$  from the three different mass bins:  $14.0 \leq \log(M/[h^{-1}M_\odot]) \leq 14.2$  (triangles);  $14.2 \leq \log(M/[h^{-1}M_\odot]) \leq 14.4$  (diamonds);  $14.4 \leq \log(M/[h^{-1}M_\odot]) \leq 14.6$  (squares). The solid lines correspond to the analytic models, Equation (10), with the best-fit parameters.

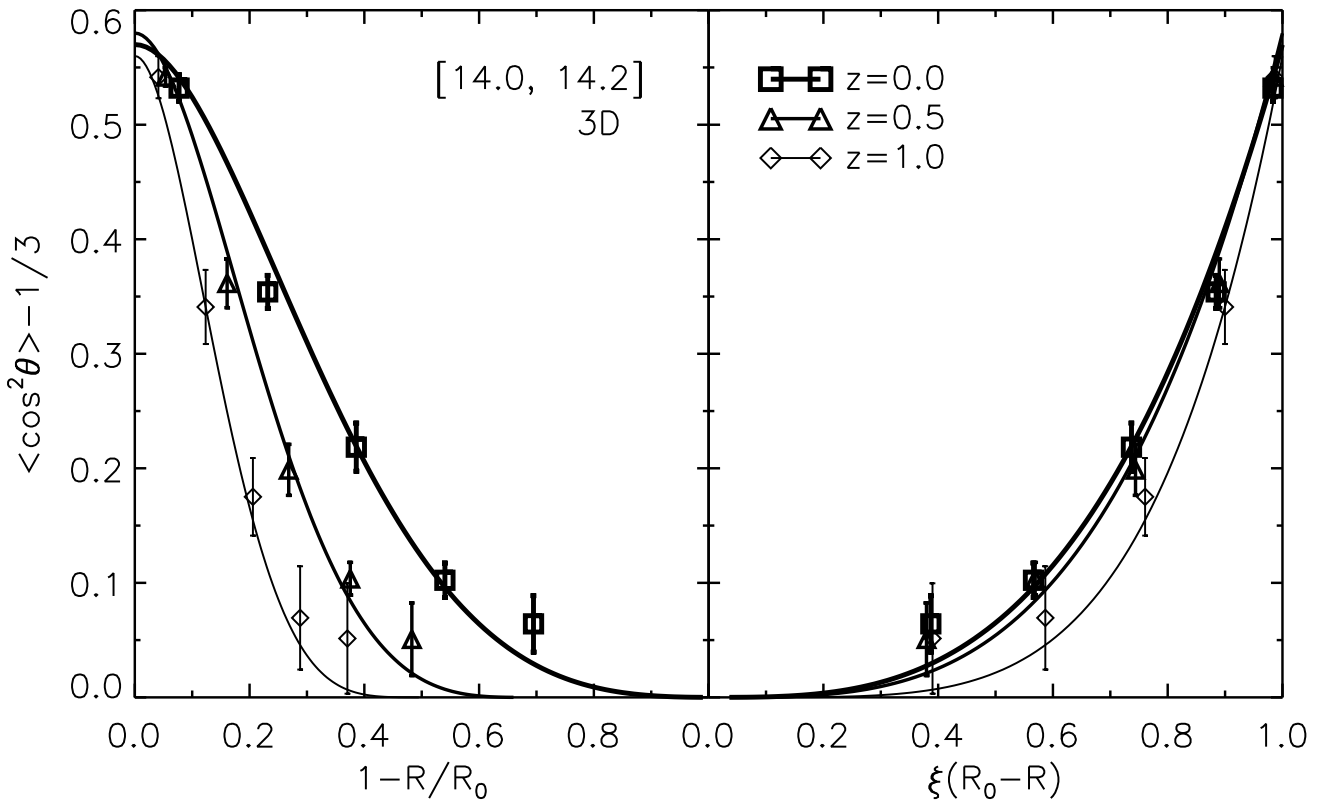


Fig. 3.— Three dimensional alignment profiles of satellite galaxies in clusters with logarithmic mass in the range of  $14.0 \leq \log(M/[h^{-1}M_{\odot}]) \leq 14.2$  at three different redshifts:  $z = 0, 0.5, 1$  (open squares, triangles and diamonds, respectively). The solid lines correspond to the analytic models, Equation (10), with the best-fit parameters at  $z = 0, 0.5$  and  $1$ , respectively.

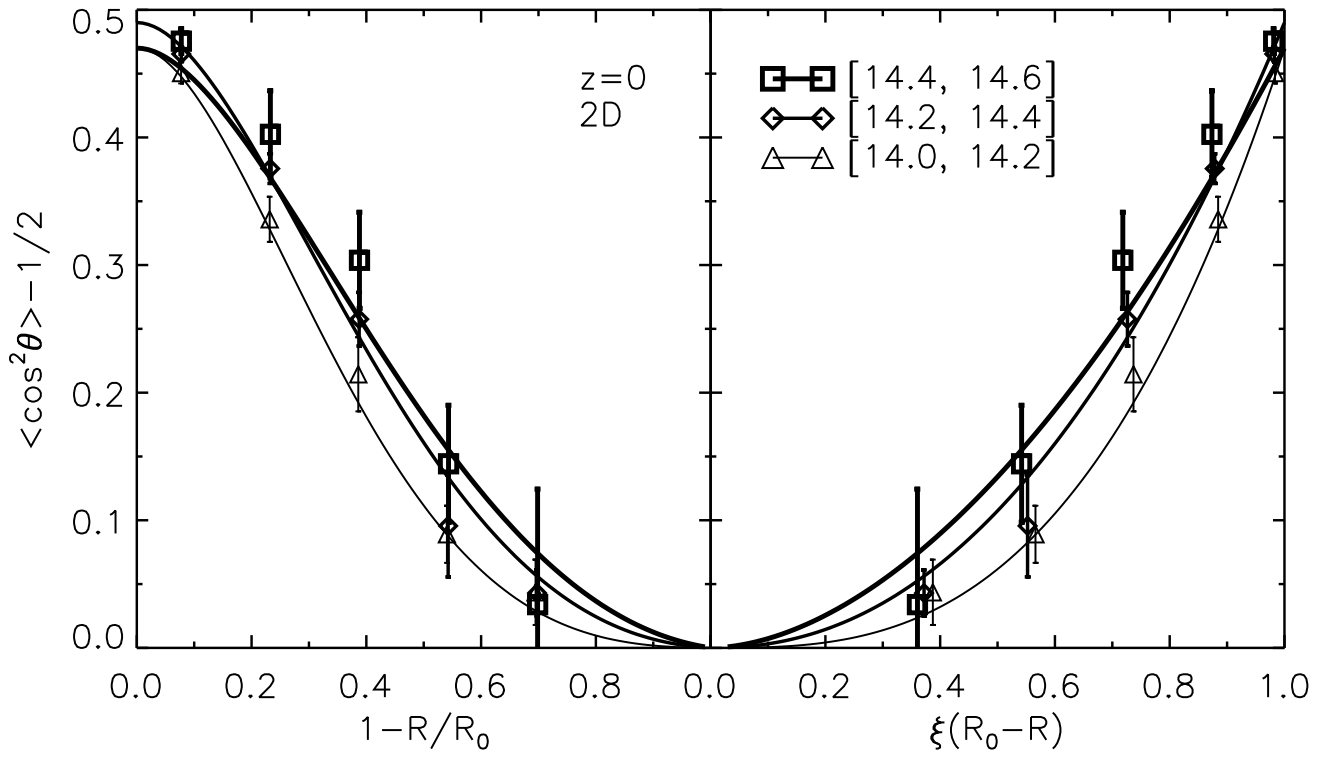


Fig. 4.— Same as Figure 2 but for the two dimensional case.

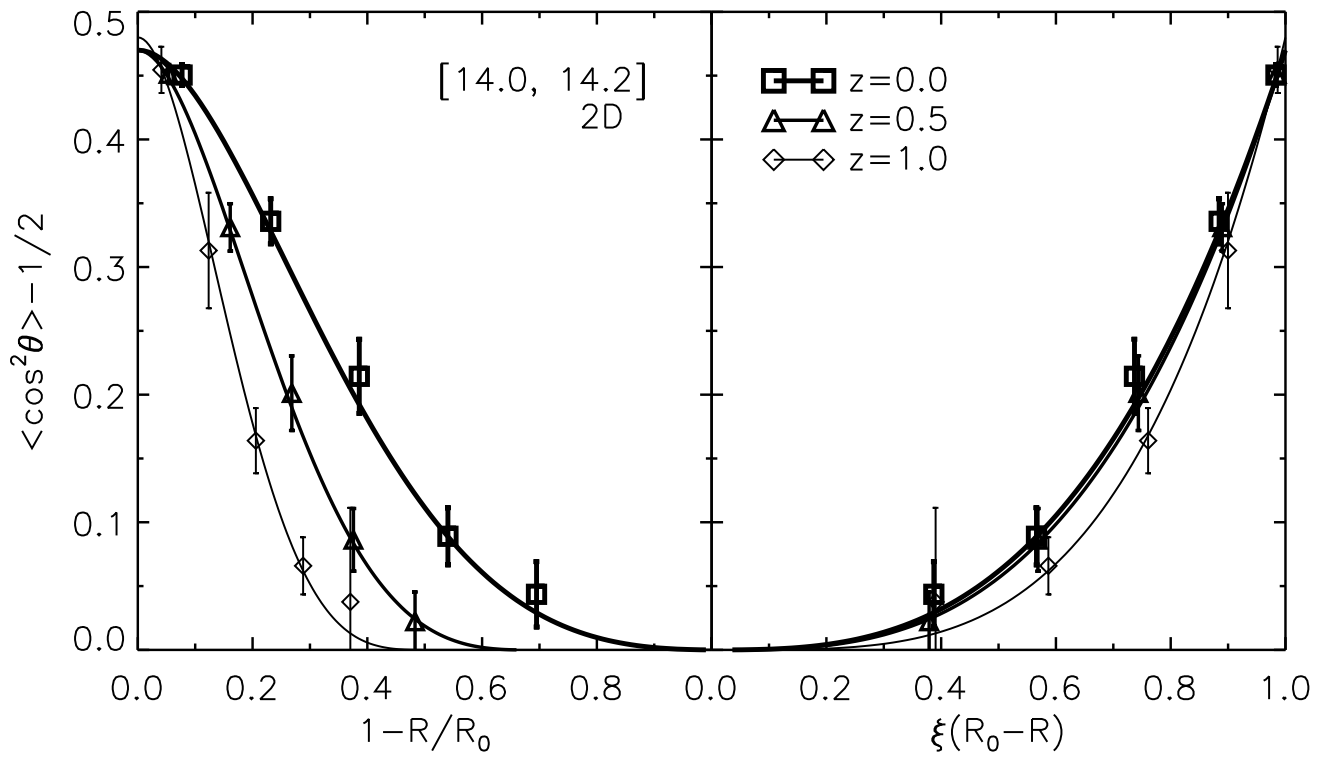


Fig. 5.— Same as Figure 3 but for the two dimensional case.

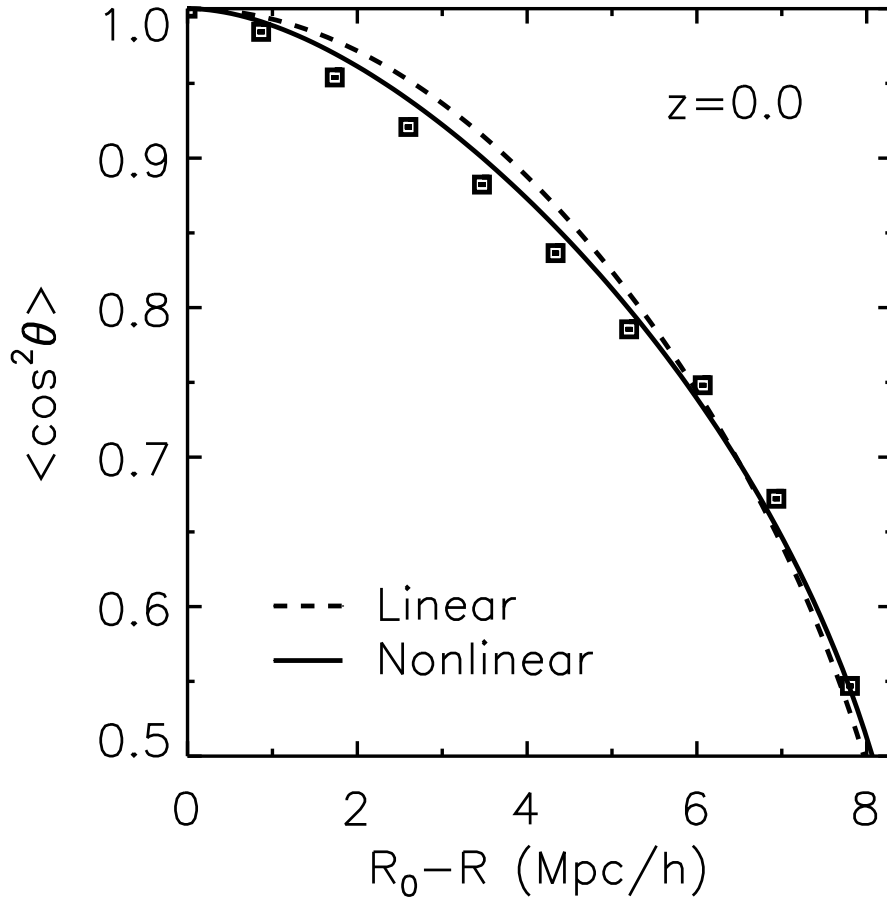


Fig. 6.— Alignments between the minor principal axes of the Millennium tidal fields smoothed on two different top-hat scales (square dots) at  $z = 0$ . The analytic models expressed as a power law of the density correlation coefficients expressed in terms of linear and nonlinear density power spectrum (dashed and solid line, respectively).

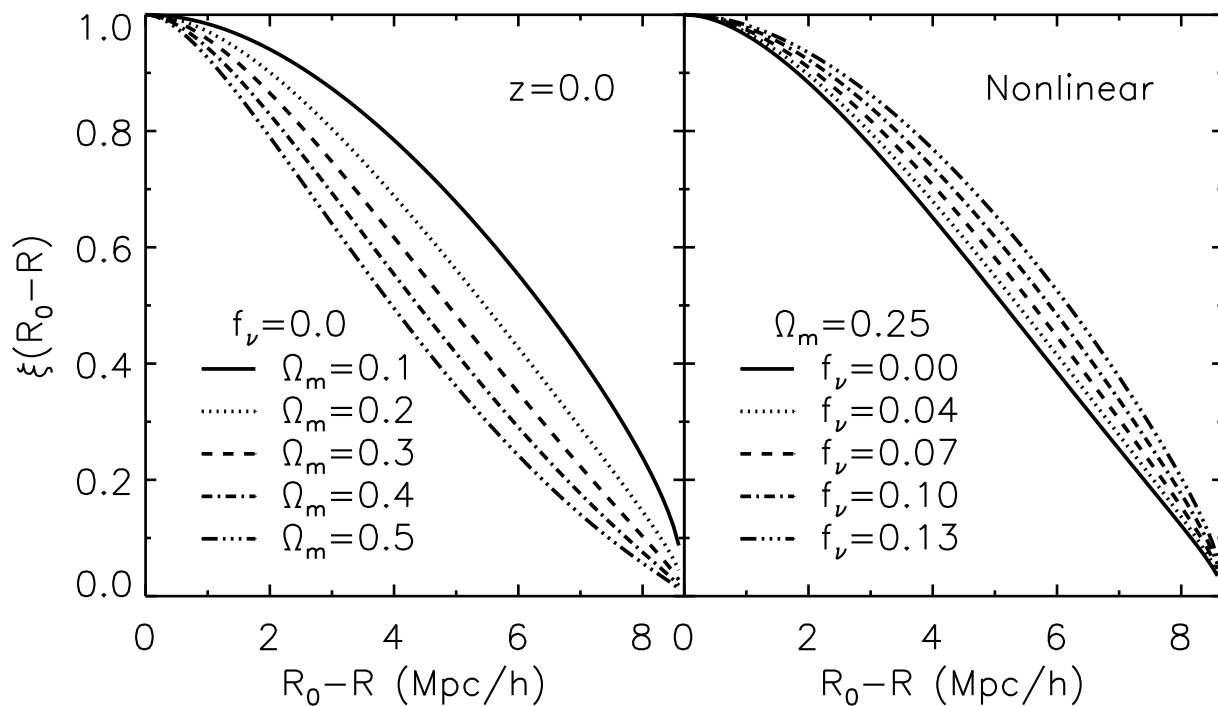


Fig. 7.— The density correlation coefficient expressed in terms of the nonlinear density power spectrum for five different values of  $\Omega_m$  and of  $f_\nu$  (left and right panel, respectively). The other key cosmological parameters are fixed at the same values as for the Millennium simulations.

Table 1. Redshift, logarithmic mass range, number of the selected clusters, best-fit amplitude, and best-fit power-law index of the three dimensional alignment profiles of satellite galaxies in the clusters from the five samples

sample	$z$	$\log(M/[h^{-1}M_{\odot}])$	$N_c$	$A$	$n$
I	0	[14.0, 14.2]	1250	$0.570 \pm 0.006$	$3.130 \pm 0.038$
II	0	[14.2, 14.4]	649	$0.600 \pm 0.010$	$2.350 \pm 0.017$
III	0	[14.4, 14.6]	337	$0.630 \pm 0.006$	$2.280 \pm 0.090$
IV	0.5	[14.0, 14.2]	832	$0.580 \pm 0.005$	$3.420 \pm 0.041$
V	1	[14.0, 14.2]	369	$0.560 \pm 0.005$	$4.700 \pm 0.042$

Table 2. Same as Table 1 but for the two dimensional alignment profiles

sample	$N_c$	$A$	$n$
I	1077	$0.470 \pm 0.004$	$2.930 \pm 0.049$
II	552	$0.490 \pm 0.001$	$2.190 \pm 0.021$
III	289	$0.470 \pm 0.004$	$1.810 \pm 0.096$
IV	724	$0.470 \pm 0.003$	$3.060 \pm 0.065$
V	324	$0.480 \pm 0.005$	$3.840 \pm 0.050$

Table 3. Result of the linear regression test of the dependence of the best-fit parameters of the alignment profiles on the logarithmic mass and redshift

function	$\alpha$
$A(\log M)$	+0.100
$n(\log M)$	–1.417
$A(z)$	–0.007
$n(z)$	+1.047